International Journal of Nanomedicine

Dovepress
open access to scientific and medical research

Open Access Full Text Article

ORIGINAL RESEARCH

Multifunctional Coating with Both Thermal Insulation and Antibacterial Properties Applied to Nickel-Titanium Alloy

This article was published in the following Dove Press journal:
International Journal of Nanomedicine

ZhiBo Liu*
KangWen Xiao*
ZhiQiang Hou
FeiFei Yan
Yan Chen
Lin Cai

Department of Orthopedics, Zhongnan Hospital of Wuhan University, Wuhan, Hubei 430071, People's Republic of China

*These authors contributed equally to this work

Background: With excellent shape memory and superelastic properties, shape memory alloy (SMA) is an ideal actuator, and it can form smart structure for different applications in medical field. However, SMA devices cause apparent thermal damage to the surrounding tissues when it works in vivo, making the application of smart structure that is composed of SMA actuator in vivo is greatly limited.

Methods: In this paper, coating (APA) with PLA as the main body to limit the heat conduction, a multifunctional Ag nanoparticles (AgNPs)/polylactic acid (PLA)/Al2O3 was synthesized. The Al2O3 layer was formed by micro-arc oxidation (MAO) and AgNPs were synthesized by silver nitrate and ethylene glycol. Scanning electron microscopy, transmission electron microscope, and Fourier transform infrared spectra were applied to analyze the morphology and characterization of APA coating. The antimicrobial activity, thermal insulation activity, and biocompatibility of APA coating were furtherly explored and verified through animal experiments and immunohistochemistry.

Results: With different particle sizes and concentrations of AgNPs, APA multi-functional films were successfully prepared. The Al2O3 layer was closely combined with SMA and formed a porous surface, so the PLA and AgNPs layers can firmly adhere to SMA, thus reducing the release of nickel ions in SMA. AgNPs gave APA coating excellent antibacterial activity and effectively inhibited the growth of Staphylococcus aureus. In addition, coupled with the low thermal conductivity of PLA and Al2O3, AgNPs were tightly anchored on the surface of PLA, which has high infrared reflectivity, making the APA coating obtain good thermal insulation performance.

Conclusion: We have successfully prepared the APA coating and obtained the optimum amount of AgNPs, which makes it have good thermal insulation performance, good antibacterial activity and good biocompatibility, which provides a new prospect for the application of SMA.

Keywords: thermal insulation, nickel-titanium alloy, silver nanoparticles, micro-arc oxidation

Introduction

With excellent shape memory effect and superelasticity, Nickel-titanium shape memory alloy (SMA) was discovered in the 1960s, and it has been widely used in aerospace, metallurgy, manufacturing, and other fields.[1] Due to its excellent and superplastic property, low magnetism, wear resistance, fatigue resistance, and excellent biocompatibility, SMA also has a wide range of applications in medical field, preparing various internal fixtures such as orthodontic archwire, U-shaped

Correspondence: Lin Cai
Tel +86 1388609 6467
Email orthopedics@whu.edu.cn

submit your manuscript | www.dovepress.com
DovePress
http://doi.org/10.2147/IJN.S266247

nail, rib claw, fibula embracing device, wrist triangle fusion cage and interbody fusion cage.[2,3] It is also widely used in vascular stents, vascular embolizers, vascular staplers, and intestinal staplers.[4,5] In medical field, SMA mainly made use of its excellent superelasticity, but, in recent years, the shape memory effect of SMA has been paid more and more attentions. With excellent material compatibility, small weight, and capability for voluntary movement, SMA is an ideal actuator and it can form a smart structure for different applications in medical field.[6] For example, driven by a SMA built into the capsule endoscope, an injection system can control its labeling and positioning in vivo and vitro.[7] There is also a bladder driver that replaces the out-of-control bladder to urinate and removes urine by extruding the bladder with the deformation of SMA.[8] Activated by electromagnetic induction heating, SMA can be implanted into penile prosthesis to replace the commonly used hydraulic-driven penile prosthesis,[9] and SMA spinal orthopedic rod for the treatment of scoliosis.[10] However, work stably in the body, all SMA devices must make the end temperature of reverse martensitic transformation to be higher than the maximum temperature of the human body, because the occurrence of shape memory of SMA is driven by temperature. Otherwise, the device could deform automatically in the body and no longer be controlled by the outside world. It is well known that, under normal circumstances, the highest temperature of human body is 42°C. When the local temperature reaches 45°C, it causes apparent thermal damage to the surrounding tissues.[11] In such a short temperature range, the application of smart structure that is composed of SMA actuator in vivo is greatly limited. Besides, release of nickel ions for SMA itself is excessive, leading to the potential danger of long-term implantation in human bodies.[2] For all medical implants, the bacterial infection is always an unavoidable problem. Implanted into the human body, the foreign bodies are priority places for microbial contamination that causes prosthesis infection and eventually the failure of implantation. Therefore, the cost of hospitalization and the anxiety and stress of patients significantly increase.[12] There are many studies on the limitation of the release of nickel ions and control the bacterial infection of implants. Many mature and feasible surface modification schemes, including alumina coating prepared by micro-arc oxidation and electroless deposited hydroxyapatite coating, can isolate the release of nickel ions. By preparing an iodine coating or nano-silver on the surface of the implant, bacterial infection is notified.[3,13,14] However, no one has ever designed a thermal insulation coating for implants that can reduce the thermal damage caused by excessive temperature during the operation of SMA. In previous studies, some researchers did not pay much attention to thermal injury,[9] while others simply covered it with silicone tubes,[15] which can not only greatly increase the volume of the implant, but also increase the risk of implant infection. As a long-term implant, its biocompatibility does not support its implantation. Therefore, a composite thermal insulation coating can greatly reduce the thermal damage caused by SMA, prevent the release of nickel ions, and control bacterial infection, so it is urgently needed.

Al2O3 has been widely utilized in the surface modification of metal biomaterials, due to its excellent wear resistance, corrosion resistance, and biocompatibility.[16] Moreover, the pure Al2O3 ceramic has a low thermal conductivity of 28–35 W·m-1·K-1.[17] It was reported that, prepared by micro-arc oxidation (MAO) with a thickness of 1.4–5 μm and a porosity of about 30%, the thermal conductivity of the anodic aluminum oxide film is as low as 1.22 W·m-1·K-1.[18] Under the combined action of thermochemistry, plasma chemistry, and electrochemistry, MAO is the method of in-situ formation of ceramic films by placing metals or their alloys, such as Ti, Mg, and Al in aqueous electrolyte solution with electrochemical method.[19] Prepared by MAO, the coating can effectively improve the corrosion resistance and wear resistance of the implant. In addition, the rough and porous surface of the coating is beneficial to the adhesion, proliferation, and growth of cells for the improvement of the biocompatibility of the implant.[20]

As a biodegradable polyester with excellent biocompatibility[21] produced from renewable resources, PLA has been widely applied to tissue fixation, wound dressing, wound closure, and surgical implants. Most importantly, the thermal conductivity of PLA is 0.183 W·m-1·K-1.[22] For human bodies, there are usually three ways of heat transfer: heat conduction, convection, and radiation.[23,24] Therefore, the qualified thermal insulation coatings should have low thermal conductivity. In terms of thermal insulation material, at a given temperature, the effective thermal insulation must reduce its unnecessary heat exchange with the surrounding environment, which is mainly carried out through the dual modes of heat conduction and radiant heat transfer.[25] With the increase of temperature, produced by thermal radiation, the proportion of heat exchange becomes higher.[26] Many kinds of

literatures have introduced the new materials of coatings or coatings that were doped with metal/metal oxide pigments. Mainly by increasing the reflectivity of infrared radiation, these new materials can achieve thermal insulation. Therefore, they are widely used in architecture, manufacturing, and chemical industry.[27–29] It is generally believed that, with high infrared radiation reflectivity, metal has good thermal insulation effect.[30] AgNPs have high infrared reflection efficiency, acid and alkali resistance, antioxidant stability, good biocompatibility, and good antibacterial activity against multidrug-resistant bacteria.[31–34] For example, previous studies proved that a silver/polylactic acid nanocomposite (Ag/PLA-NC) film showed excellent antibacterial effect on wound dressing.[20] Bacterial infection is the most common complication of implants in vivo, so it is important to reduce the incidence of infection, inhibit the formation of biofilm and remove multi-drug-resistant bacteria. Silver-containing nanocomposites indicated great antibacterial activity and can inhibit the formation of biofilm, suggesting that it is a good antibacterial material.[35,36] But it is worth noting that, in the application of medical devices, the risks of nano-materials, including nano-silver, are still not thoroughly explored. In the case of nano-silver, what extent the intact AgNPs themselves can enter human bodies is still unclear that, and if the Ag ions released from the NPs absorbed, whether the AgNPs undergo changes in the physiological environment.[37,38] The exposure dose, particle size, coating, and aggregation state of the AgNPs, as well as the cell type or organism were tested, and are all large determining factors on the effect and potential toxicity of AgNPs. A high exposure dose to AgNPs alters the cellular stress responses initiates cascades of signaling, thus eventually triggering organelle autophagy and apoptosis.[39] Furthermore, different concentration and particle sizes of AgNPs have different effects on the infrared reflection ability and antibacterial effect of AgNPs. In order to achieve a perfect balance between thermal insulation and antibacterial effect and to reduce the cytotoxicity of AgNPs as much as possible, it is necessary to evaluate the AgNPs with different particle size and concentration.

The exploration of the minimum dosage of AgNPs can effectively resist bacteria and thermal insulation.

In this study, a novel multifunctional coating, including porous Al2O3 and PLA composites with AgNPs (APA multifunctional coating), was synthesized. Prepared by MAO, the corrosion resistance and wear resistance of porous Al2O3 effectively reduced the biotoxicity of SMA that was caused by excessive nickel ions. What is more, the porous surface enabled AgNPs and PLA composites to cover the surface of SMA firmly. Containing a large amount of AgNPs, PLA composite not only improved the antibacterial effect, but also reduced the thermal damage that was caused by the thermal drive of SMA for its high infrared radiation reflection and low heat conduction. Besides, animal experiments and immunohistochemistry were used to explore the biocompatibility of our multifunctional coating. Multi-functional APA film can reduce thermal damage, nickel ion toxicity, and infection rate, and maximize the protection of human tissues in the application of SMA, making the application of smart structure composed of SMA actuator in vivo possible and providing a broader application prospect for SMA. The schematic diagram of the overall study is illustrated in Figure 1.

Materials and Methods

Materials

Silver nitrate (AgNO3, molecular weight = 170D) was obtained from Sinopharm Chemical Reagent Co., Ltd., Shanghai, China. Polylactic acid (PLA) and Polyvinyl pyrrolidone ((C6H9NO)n) were purchased from Shanghai Macklin Biochemical Co., Ltd., Shanghai, China. Staphylococcus aureus (S. aureus) were obtained from the American type culture collection. Dichloromethane (CH2Cl2, molecular weight = 85D) Ethylene glycol (C2H6O2, molecular weight = 62D) was obtained from Sinopharm Chemical Reagent Co., Ltd, Shanghai, China. Luria Bertani Broth (LB broth) was purchased from Dalian Meilun Biotechnology Co., Ltd, China. New Zealand experimental rabbits were purchased from Wuhan WQJX Bio-Technology Co., Ltd, China. Commercial nickel-titanium alloy received from ChuanMao Suzhou Metal material Co., LTD, China, was also used in this study.

Micro Arc Oxidation on a Nickel-Titanium Alloy

The MAO was conducted by an MAO equipment (Multifunctional single - and bidirectional pulse composite micro-arcs oxidation power supply, DSM30F) from Harbin Disi numerical control co., Ltd, China. The electrolyte solution consisting of 0.15M NaAlO2 and 0.03M NaH2PO2·H2O. Nickel-titanium alloy samples were used as anodes, while spiral steel tubes were used as the cathode (Duty cycle =30%, constant forward current =12A,

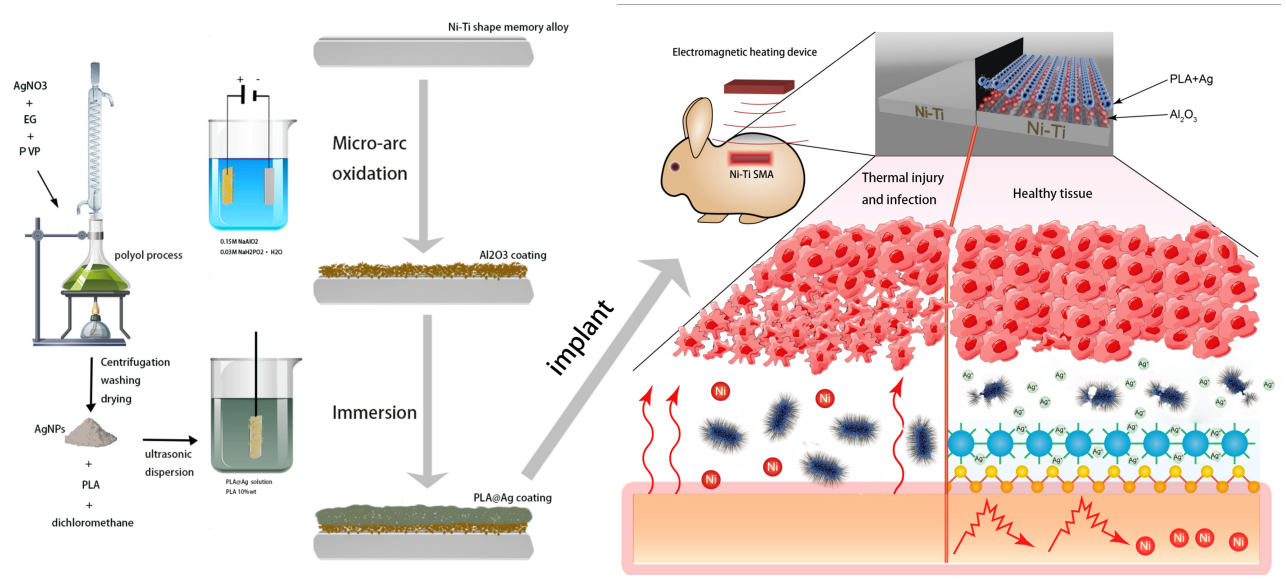

Figure 1 Schematic diagram of the overall study.

constant reverse current =4A, constant forward voltage =420V, constant reverse voltage =75V). The process lasted for 30 minutes, and the temperature of the electrolyte solution was below 30°C.

Synthesis of Ag Nanoparticles/PLA Membrane

AgNO3 and PVP were dissolved in ethylene glycol. The solution was stirred vigorously in a reactor equipped with a reflux condenser. Besides, the solution was further heated at 100–150°C with a constant heating rate of 1–7.5°C min-1. Each reaction lasted for 30 minutes based on the different heating rate and reaction temperature. Finally, the AgNPs with different nanosize were collected by centrifugation and repeatedly cleaned by deionized water. Then the AgNPs were dissolved in dichloromethane solution containing 10 wt% PLA. The mixture was stirred in an ice bath for 2 hours, avoiding light. The Ag/PLA membranes were prepared by solvent casting, which was a conventional method for membrane fabrication.[40] The solution was poured into a mold and placed in a drying oven at 100°C for 6 h for evaporation. The completely dried membrane was obtained and cut into the desired forms. Ag/PLA membrane with different Ag concentrations (m/v=0.1, 0.2, 0.3, 0.4g/L) were obtained by changing the ratio of AgNPs/dichloromethane/PLA. Ag/PLA membrane with different particle sizes (D= 1,040,100) was also obtained by changing the size of AgNPs. These membranes are mainly used for antibacterial and thermal insulation experiments. The SMA coated with Al2O3 layer was completely immersed in the mixture for 2 hours. Then the nickel-titanium alloy rod was taken out and placed in a drying oven at 100°C for 6 hours, SMA coated with APA multifunction composite film was obtained for follow-up experiments.

Material Characterization

Field emission scanning electron microscopy (JSM-7800F FESEM, Japan) and transmission electron microscope (HITACHI H-7000FA, Japan) were performed to analyze the morphological characteristics of the Ag/PLA membrane. The crystallography of the Ag/PLA membrane was characterized by X-ray diffraction (XRD) analysis by BRUKER D8 ADVANCE, Germany. Besides, functional groups of the film were identified by Fourier transform infrared spectra (FTIR) by Thermo Nicolet 6700, USA. Furthermore, the particle size distribution of samples was measured by a submicron size analyzer (Mastersizer 3000, UK).

Antimicrobial Activity Test

To explore the antibacterial properties of PLA films containing different sizes and concentrations of AgNPs, we divide the PLA@Ag films into 8 groups, including blank control and PLA, PLA@0.2Ag, PLA@0.3Ag, PLA@0.4Ag, PLA@20Ag, PLA@50Ag, PLA@100Ag.PLA@0.2Ag, PLA@0.3Ag, and PLA@0.4Ag, respectively. PLA@0.2Ag,

PLA@0.3Ag, PLA@0.4Ag represented PLA films with 20nm AgNPs at concentrations of 0.2 wt%, 0.3 wt%, and 0.4 wt%, respectively. PLA @ 20Ag, PLA @ 50Ag, PLA @ 100Ag represented PLA films at 0.3wt% AgNPs with particle diameters of 20nm, 50nm, and 100nm, respectively. Each group was made into films with Φ10*0.3 and placed at the bottom of a 12-well plate. Gram-positive bacteria S.aureus was chosen as an experimental bacterial, and LB broth was used as a culture medium. The bacteria were diluted in LB broth to 107colony-forming units (CFU)/mL, and the diluted bacterial solution with 400ul was added to the 12-well plate of PLA film containing different sizes and concentrations of AgNPs. The inoculated bacteria were cultured for 8 hours at 37°C for 24 hours. The bacterial concentrations of each group at different time points were analyzed and measured at 620 nm using a spectrophotometer Enzyme Immunoassay Analyzer (Perkin Elmer Enspire 2300, USA). To facilitate the expression of the bacteriostatic activity was appraised by the following equation:

Bacteriostatic rate (%) = (A - B)/A × 100%

where A is the OD value of the blank control, and B is the OD value of a given sample. Besides, to directly reflect the antibacterial effect of each group, the bacterial solution of each group cultured for 12 hours was diluted 10,000 times, the diluted bacterial solution of 50ul was added to the blood Agar petri dish and smeared evenly with a push rod, and the blood Agar petri dish was cultured at 37°C for 24 hours. Then, we took out the plate to take pictures and count the colonies.[41]

To explore the difference of the antibacterial effect of PLA films containing different concentrations of 20nm AgNPs at different temperatures (37°C, 41°C, 45°C, 49°C), blank control group, PLA, PLA@0.1Ag, and PLA@0.2Ag groups were used. The diluted bacterial solution of 400ul was added to 12-well plates containing different groups of films and cultured in an incubator at 37°C for 4 hours, and then heated in a constant temperature water bath pot for 8 hours. The temperature of the water bath pot was set to 37°C, 41°C, 45°C, and 49°C. Stained with L13152 living bacteria viability kit (L13152, American molecular probe), the living bacteria and dead bacteria were distinguished and photographed under a fluorescence microscope. In order to further explore the specific reasons for the antibacterial effect of each group, put different groups of films into a 12-well plate as in the previous step, and then add the bacterial medium of 200ul, then heated in a constant temperature water bath pot for 8 hours. The temperature of the water bath pot was set to 37°C, 41°C, 45°C, and 49°C. The diluted bacterial solution of 200ul was added to 12-well plates and cultured in an incubator at 37°C for 12 hours. To investigate the regularity of ion release, the PLA@Ag film samples were immersed in PBS solution for 0.5, 1, 4, and 7days (solution volume to sample mass: 200 mL/g). The concentrations of Ag ions were measured by inductively coupled plasma atomic emission spectrometry (ICP-AES, IRIS Intrepid II XSP, Thermo Fisher). All experiments were triplicate.

Thermal Insulation Test

The purpose of this study was to explore the thermal insulation effect of PLA films containing different sizes and concentrations of AgNPs, and the principle of different thermal insulation effects. Therefore, 8 groups, including blank control and PLA, PLA@0.2Ag, PLA@0.3Ag, PLA@0.4Ag, PLA@20Ag, PLA@50Ag, PLA@100Ag were used. Each group was made into a film withΦ10*0.3. Put the films in a constant temperature water bath at 50 degrees Celsius. The thermal images of the experimental group were taken by Thermal imager (FLIR X6900sc SLS, USA) and the temperature changes were recorded. Then, Infrared emission rates and thermal conductivity of every sample were measured by FLASHLINETM3000 (ANTER Corporation, USA) and UV-2700 Ultraviolet-visible Spectrophotometer (SHIMADZU, Japan), respectively. To investigate the thermal insulation effect of alumina coating prepared by MAO, we selected one piece of NiTi SMA with 20*20*1mm size, and one piece of NiTi SMA coated with alumina film of the same size. Put it in a constant temperature water bath at 45°C. The thermal images of the experimental group were taken by Thermal imager (FLIR X6900sc SLS, USA) and the temperature changes were recorded.[42]

To explore the thermal insulation ability of the complete multifunctional film, we used agarose gel solid medium in vitro to simply simulate the environment of animals in vivo. The memory alloy rod with a length of 5cm and a diameter of 3mm and a memory alloy rod covered with a complete multifunctional film were implanted, respectively, and the memory alloy rod was heated externally by an electromagnetic heating device. Finally, thermal images of each sample were obtained by Thermal imager (FLIR X6900sc SLS, USA). All experiments were triplicate.

In vitro Biocompatibility

To test cell viability, murine fibroblasts (L929) purchased from American type culture collection were used and cultured 8.0 × 103 on each well of a 96-well plate for 24 h (per well, 200uL medium). Then, we added 0.2mL fresh medium with modified DMEM medium, 10% fetal bovine serum (Gibco, USA),1% penicillin (Gibco, USA), and 1% streptomycin (Gibco, USA), and after incubation in 95% air humidity and 5% CO2 at 37°C for 1, 3 and 5 days. The modified DMEM medium was prepared as follows: all types of samples under ultraviolet radiation sterilization were prepared. Those samples including PLA, PLA@20Ag, PLA@Ag@NiTi and NiTi were soaked in DMEM medium at a rate of 3cm2/mL according to ISO/EN 10,993–5 standards and incubated at 37°C for 48h. At the given time points, the viability of the cells was determined by the Cell Counting Kit-8 (CCK-8) assay, and the optical density of each well was measured at 450 nm using a spectrophotometer Enzyme Immunoassay Analyzer (Perkin Elmer Enspire 2300, USA) to indicate cell viability. All experiments were triplicate.

To evaluate attachment and morphology of L929s in different PLA film samples, 2.0 × 104 L929s were seeded in the PLA, PLA@20Ag PLA film samples, respectively. After L929s were cultured for 2 hours, 1 day and 3 days, the PLA film samples were incubated with 4% paraformaldehyde for 20min, and washed with PBS three times and then stained with FITC (Sigma-Aldrich, USA) for 20min. Followed by washing with deionized water 3 times, and cellular nuclei were stained with DAPI for 5min and observed under a confocal laser scanning microscope.

The Animal in vivo Experiment

New Zealand experimental rabbits were used in this experiment. All animals were raised at controlled temperature (22–26°C), 12-hour light period and 12-hour dark period with appropriate food and water. The Zhongnan Hospital approved the surgical procedures and treatment with animals of the Wuhan University Ethics Committee. All animals were treated by following China Public Health Service Guide For the Care and Use of Laboratory Animals. Rabbits were randomly divided into 3 groups: PLA@Ag@NiTi, NiTi and sham-operated control by exposing wound without any treatment. The rabbits were anesthetized by inhaling Isoflurane with 0.4 concentration at a constant rate and further immobilized and shaved. The surgical area was disinfected with iodine. Implants were placed intramuscularly near the spine of the rabbits, and the temperature measurement was then fixed to the Niti surface with an optical fiber thermometer to measure the temperature change. The wound was sutured with nylon monofilaments, and penicillin was administered to prevent post-operation wound infection. X-ray images were obtained after the operation of each rabbit by the Zhongnan Hospital. Three days after the operation, the SMA rods in rabbits were heated by an electromagnetic heating device. Under the monitoring of optical fiber thermometer and ensuring that the electromagnetic heating device was fixed at the same heating power and heating distance, each group was turned on for 120s. The whole blood and surrounding tissue of implants from each rabbit were obtained after 15 days of surgery for histopathological analysis. The tissue was immobilized by a 10% methanol solution (beyotime, Shanghai), then dehydrated with ethanol and embedded in paraffin. Transverse sections of the tissue were obtained and stained with hematoxylin and eosin. Immunohistochemistry was also performed on this tissue. Histopathologic changes of the tissue were examined under optical microscopy (Aperio VERSA 8, Germany) by an experienced pathologist in a blinded fashion.

Statistical Analysis

SPSS 16.0 software was used for statistical analysis. All data were presented as mean ± standard deviation (x ± s) and analyzed by one-way ANOVA. The significant difference was considered when the $P < 0.05$.

Results and Discussion

Morphology and Characterization of Multifunctional Coating

Learning from the previous research experiences on the Synthesis of AgNPs with different shapes and particle sizes,[43] we successfully synthesized AgNPs with relatively narrow particle size distribution to meet the requirements of our follow-up experiments. With different particle sizes (20nm, 50nm, 100nm) displayed by transmission electron microscopy, AgNPs are shown in Figure 2A–C. In Figure 2A, the 20nm AgNPs were spherical shape and distributed evenly. Figure 2B and C displayed the 50nm and 100nm AgNPs, respectively. Moreover, Ag particle size distribution analysis is demonstrated in Figure 2D. The 20nm AgNPs sample exhibited narrow distribution around

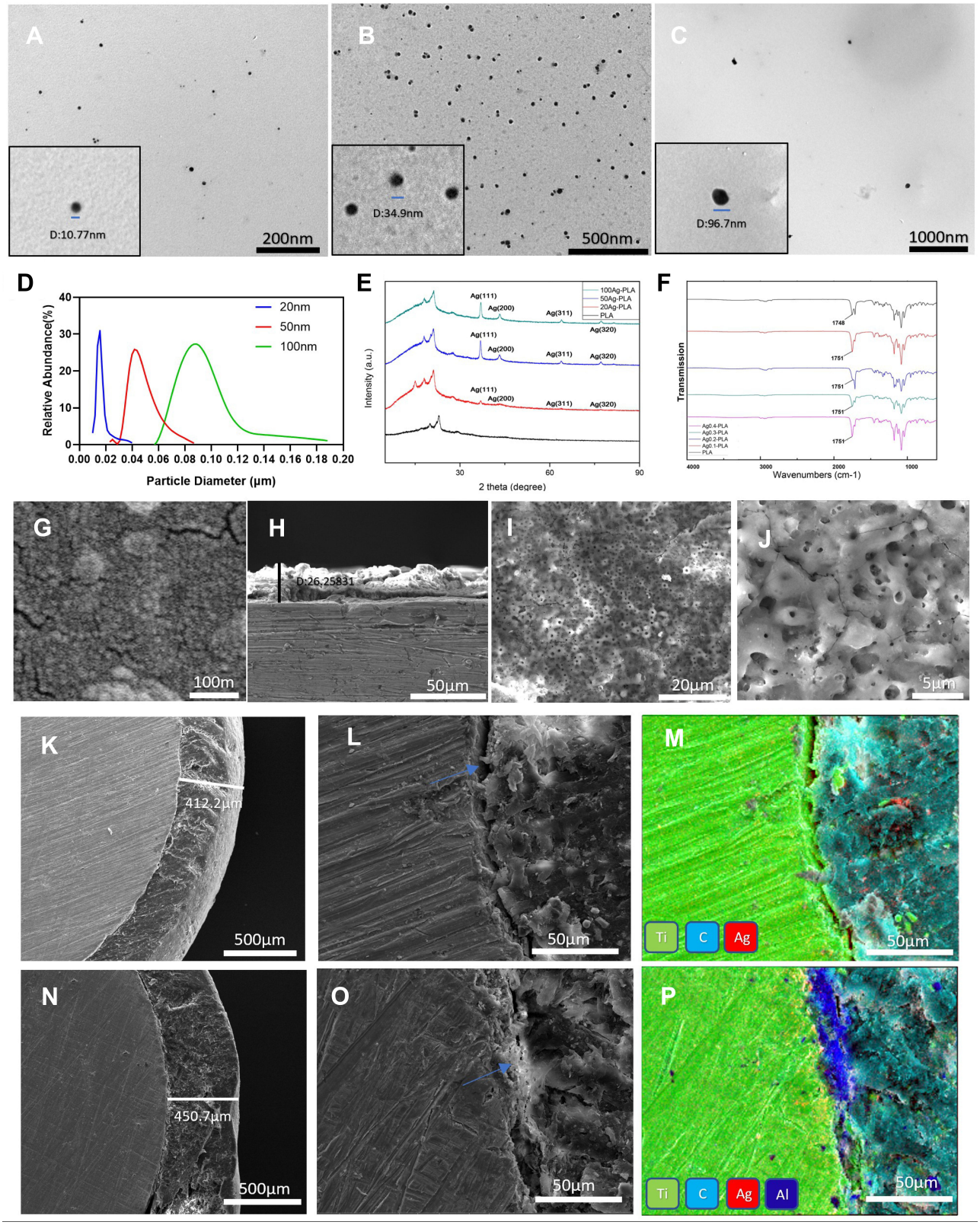

Figure 2 Morphology and characterization of APA multifunctional coating. (**A**–**C**) TEM diagrams of AgNPs with different particle sizes (10.77nm, 34.9nm, 96.7nm). (**D**) Ag nanoparticle size distribution analysis. (**E**) The crystallography of PLA@Ag film characterized by X-ray diffraction (XRD) analysis. (**F**) Fourier transform infrared spectra for PLA@Ag film with different nanosize. (**G**) SEM image of AgNPs dense distribution on the APA multi-function coating surface. (**H**) The cross-sectional SEM image of NiTi alloy rods after MAO processes. (**I, J**) The porous and rough surface of NiTi alloy rods after MAO processes. (**K**–**M**) The cross-section of APA multi-function coating without the Al2O3 layer. (**N**–**P**) The cross-section of APA multi-function coating with the Al2O3 layer.

20nm. In the 50nm AgNPs sample, the size distribution was also narrow around 50nm. In the 100nm AgNPs sample, the size distribution varied from 60 to 180nm. Besides, with different Ag concentrations ranging from 0.1 to 0.4wt%, the crystallography of Ag@PLA film was characterized by X-ray diffraction (XRD) analysis. The results are given in Figure 2E. Compared with the PLA film, three crystalline peaks were found at 38.7° (2θ), 44.8° (2θ) and 78.1° (2θ). Those additional peaks were attributed to (2 0 0), (2 2 0), and (3 1 1) crystallographic planes of face-centered cubic phase of the AgNPs.[44] What is more, in the Ag/PLA, the diffraction peaks of PLA decreased because of the presence of Ag@PLA film on the surface of PLA. The XRD results gave information that the characteristic peaks of PLA and AgNPs were apparent and no different peaks, indicating that the ideal PLA@Ag film was successfully prepared by uniformly combining pure AgNPs in the polymer structure of PLA. Then, containing different Ag concentrations ranging from 0 to 0.4g/L, functional groups of the Ag@PLA film was identified by Fourier transform infrared spectra, and the results are displayed in Figure 2F. The -CH bending was located at 1448cm-1 in PLA.[45] The carbonyl peak in PLA was observed at 1748cm-1. The -OH bending was illustrated at 3370cm-1 with a broader peak because of the van der Waals interactions between AgNPs and hydroxyl group.[46] C-O peak was observed at 1043cm-1, and the C-OH was demonstrated in 1313cm-1. In the Ag@PLA film, the carbonyl peak shifted between 1748cm-1 and 1751cm-1 due to the interactions between AgNPs and carbonyl groups. Moreover, the absence of a new peak in Ag/PLA film revealed the physical adhesion between AgNPs and PLA. With AgNPs, the morphological characterization of synthesized Ag/PLA film was furtherly observed by scanning electron microscopy and the results are exhibited in Figure 2G. The PLA film was tightly bonded to the alloy surface, the surface of the PLA was smooth, and the reticular structure made it easier to anchor the AgNPs. The AgNPs were densely deposited on the surface of the PLA for the formation of AgNPs infrared radiation reflection layer, which can improve the infrared reflection ability of PLA@Ag film.

Previous studies revealed that, after the MAO process, SMA exhibited the improvement of the surface properties of SMA.[47,48] Therefore, in this study, a layer of Al2O3 was successfully prepared on the surface of SMA by MAO. SEM images illustrated that the Al2O3 layer was about 26.26 microns thick, which was tightly bonded to NiTi-SMA and made the surface of SMA rough and porous, thus making it easier for organic polymers to bond and prevent shedding (Figure 2H–J). Without the Al2O3 layer, the microstructure of PLA@Ag- coated SMA rods are shown in Figure 2K–M, while the PLA@Ag- coated SMA rods with Al2O3 layer are demonstrated in Figure 2N–P. SEM revealed that the Al2O3 layer was tightly attached to the SMA surface. Treated by MAO, the NiTi SMA had a close bond with the PLA@Ag layer, while there was an apparent gap between the simple NiTi SMA layer and the PLA@Ag layer, indicating that the alumina layer was closely combined with the PLA@Ag layer to make the APA multi-functional coating as a whole and tightly bonded to the SMA surface. So far, we have successfully prepared the high-quality APA multi-function coating for subsequent experiments.

The Antibacterial Properties of Different PLA@Ag Films

After co-culture with the bacterial solution for 4, 8, 12, and 24 hours, the bacterial concentration of each group is displayed in Figure 3A–D. In the early stage of co-culture, the antibacterial activity of AgNPs with different particle size was significantly different. The larger the particle size was, the weaker the antibacterial activity was. The antibacterial activity was enhanced with the increase of the concentration, regardless of the AgNPs size. Moreover, after 24 hours of co-culture with bacterium, the antibacterial activity of the control group did not change significantly. In the late stage of the co-culture with the bacterium, containing a low concentration of AgNPs, the antibacterial activity of PLA films decreased significantly as time went on. Specifically, after 24 hours of co-culture with bacterium, containing 0.1wt%, 0.2wt%, 0.3wt% and 0.4wt% AgNPs with 20nm particle size, the antibacterial activity of PLA film was 8.14%, 9.31%, 89.53%, and 96.86%, respectively. When the concentration of AgNPs ≥0.3wt%, the PLA@Ag film showed excellent antibacterial activity. When the concentration ≤0.3wt%, it almost displayed no antibacterial activity. Besides, for AgNPs at the same concentration, PLA films containing 20nm AgNPs exhibited better antibacterial activity. The specific results were as follows: after 24 hours of co-culture with the bacterium, the antibacterial activity of PLA thin films that contains 20nm, 50nm, and 100nm AgNPs with a concentration of 0.3wt% was 89.53%, 36.51% and 33.58%, respectively (Figure 3C and D). The antibacterial

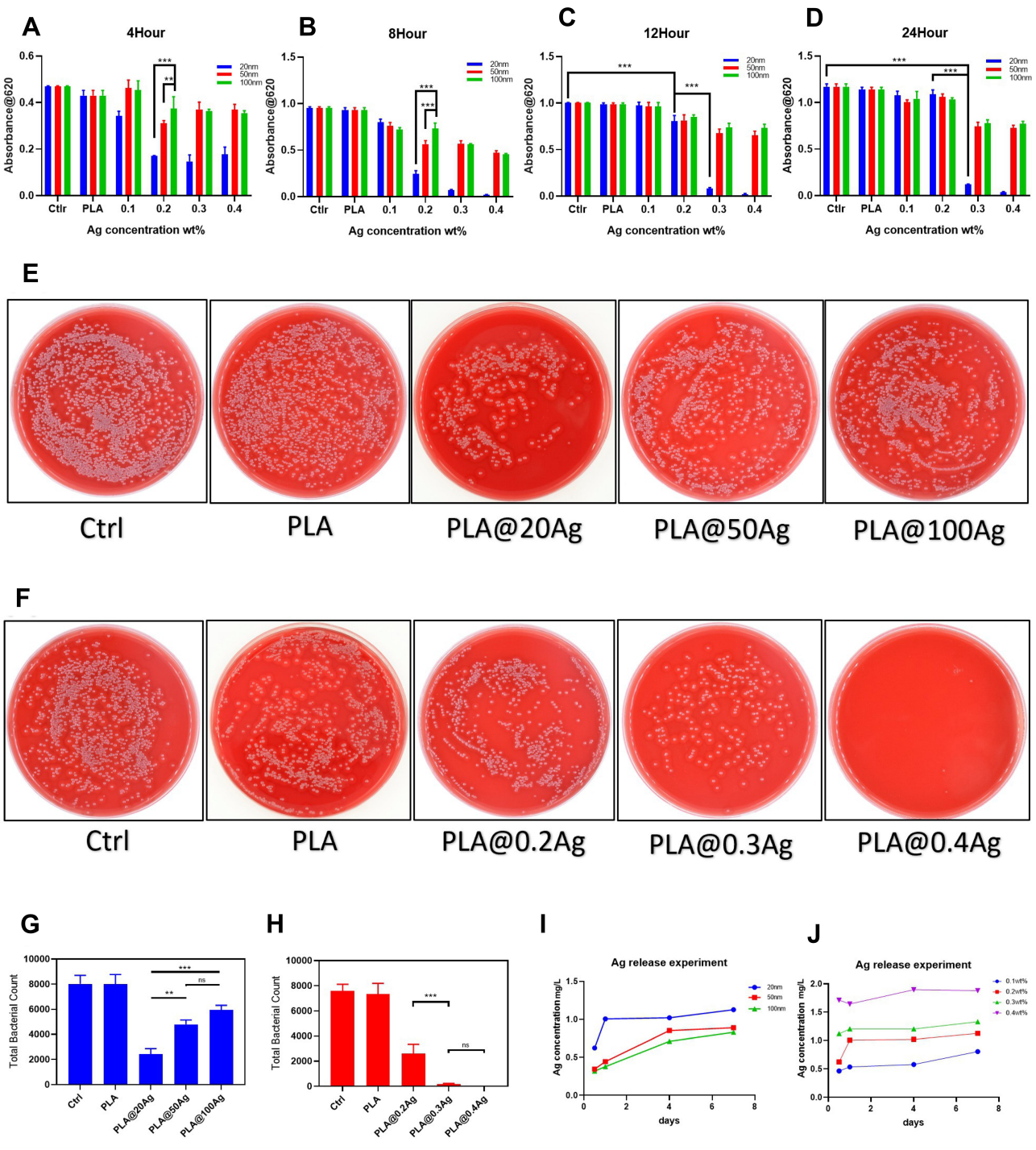

Figure 3 Antibacterial properties of APA multifunctional coating. (**A**–**D**) UV absorption spectrum at 620nm of bacterial liquid co-culture with different PLA@Ag film for 4h, 8h, 12h and 24h, respectively. (**E, F**) Growth of bacteria in different concentrations and nanosize of AgNPs on blood agar at 12h. (**G, H**) Total bacterial count for PLA@Ag film with different Ag nanosize and concentration. (**I**) Ag release experiment for PLA@Ag film with different Ag nanosize (20nm, 50nm, 100nm). (**J**) Ag release experiment for PLA@Ag film with different Ag concentration (0.1wt%, 0.2wt%, 0.3wt%, 0.4wt%). **p< 0.02, ***p< 0.001.

activity of PLA@Ag film was furtherly explored by spread plate method (SPM) using a blood plate, because turbidimetric test could not distinguish the live and dead bacteria. The results of SPM are shown in Figure 3E and F. As displayed in Figure 3G and H, we made a quantitative analysis of the colonies of each blood plate, the trend was consistent with the results of the above turbidimetric test.

Based on the results of early silver ion release experiments, the silver ion release ability of smaller AgNPs was higher than that of larger AgNPs. Released by

PLA@50Ag and PLA@100Ag groups that were soaked for 24 hours, the silver ions were 0.441±0.019mg/L and 0.372±0.007mg/L, respectively, while those in PLA@20Ag group were 1.017±0.019mg/L (Figure 3I). Besides, with the increase of the concentration of AgNPs, the amount of silver ion release also increased (Figure 3J), corresponding to the above antibacterial results. It is well known that Ag has a disinfection effect and is used to treat burns and chronic wounds in traditional medicine.[49] As in previous studies, AgNPs had excellent antibacterial activity. Adding AgNPs to polymer materials such as PLA could improve excellent antibacterial activity, but pure PLA films without AgNPs had no antibacterial activity.[50–52] In this research, we carried out a large number of experiments, and the results revealed that AgNPs, with higher concentration and smaller particle size, had better the antibacterial effect. In terms of antibacterial activity, the antibacterial activity of Ag was related to the amount and the release rate of Ag ions.[53] The different concentration and particle size of AgNPs in PLA films lead to different antibacterial activity of Ag ions from the PLA matrix, and this may be ascribed to the release. Ag is inert in its mental state, but when it comes to contact with body fluids, it ionizes and releases silver ions. Ionized silver has extremely high activity. First, Ag ions bind strongly to electron donor groups in biological molecules, including sulfur, oxygen, or nitrogen, causing defects in the bacteria cell wall, so cell contents are lost, thus leading to the death of the bacterial cells. Secondly, it also binds to DNA or RNA of bacteria and finally inhibits bacterial replication.[54] Therefore, the particle size of AgNPs mixed in PLA is less than 20nm to make the new multifunctional coating have a stable antibacterial effect, and the concentration is more than 0.3wt%.

Effect of Temperature on Antibacterial Property of APA Multifunctional Coatings

In order to explore whether the heat absorbed by the multifunctional coating during thermal insulation could improve the antibacterial effect, with different concentrations at different temperatures, we performed the antibacterial experiments of PLA films containing 20nm AgNPs, and the results are illustrated in Figure 4A. The results of the turbidimetric test indicated that the removal of AgNPs did have a 25.53% antibacterial activity at 49°C. However, the experimental groups with lower temperatures, such as 41°C and 45°C, had no inhibitory effect on S. aureus. It can be seen that the effect of temperature on bacteria at 49°C is very slight and can not play a role in bacteriostasis. After adding the PLA@Ag composite film, the situation changed. At average culture temperature 37°C, the antibacterial activity of PLA@Ag composite film was not ideal. The antibacterial activity of PLA@0.1Ag and PLA@0.2Ag was only 44.16% and 60.86%, respectively, but they increased to 88.75% and 93.42% at 49°C. We designed an experiment to remove the effect of temperature difference in the culture environment to explore the reason, and the results are shown in Figure 4B. It can be seen that although it was cultured at 37°C for 12 hours, the antibacterial activity of both PLA@0.1Ag group and PLA@0.2Ag group after pretreatment at 49°C was significantly higher than that of the control group pretreated at 37°C. Therefore, in order to verify this conjecture, Ag ion release experiments at different temperatures were performed, and the results are shown in Figure 4C. Released by the PLA@0.2Ag group soaked at 37°C, 41°C, and 45°C for 24 hours, the release of Ag ion did increase with the increase of temperature. It can be inferred that the release of more silver ions caused by higher temperature during pretreatment increased the antibacterial activity of the experimental group. Staining methods were used to distinguish live and dead bacteria to illustrate this effect more intuitively, and the results are demonstrated in Figure 4D. The overall trend was similar to the above results. PLA@0.2Ag group displayed good antibacterial activity under the synergistic action of high temperature. The PLA@0.2Ag group soaked in the ambient temperature of 37°C, 41°C, and 45°C for 24 hours. It could be seen that the higher the ambient temperature was, the more Ag ions were released. Compared with 37°C, the ability of the composite membrane to release silver ions was promoted at 49°C. This result well explained the difference in antibacterial effect at different temperatures. In past decades, non-contact metal implantation induction heating has become a new method for the treatment of metal implant infection. For example, electromagnetic heating was used to heat metal implants to 60°C to kill bacteria by removing surface biofilm. However, serious complications such as tissue thermal injury and bone loss happened,[55] because the operating temperature was too high and difficult to control. Our APA multifunctional coating solved the above problems by greatly improving antibacterial and thermal insulation effect. After adding APA multifunctional coating, the antibacterial activity in the environment of 49°C was significantly improved to 93.42%. More

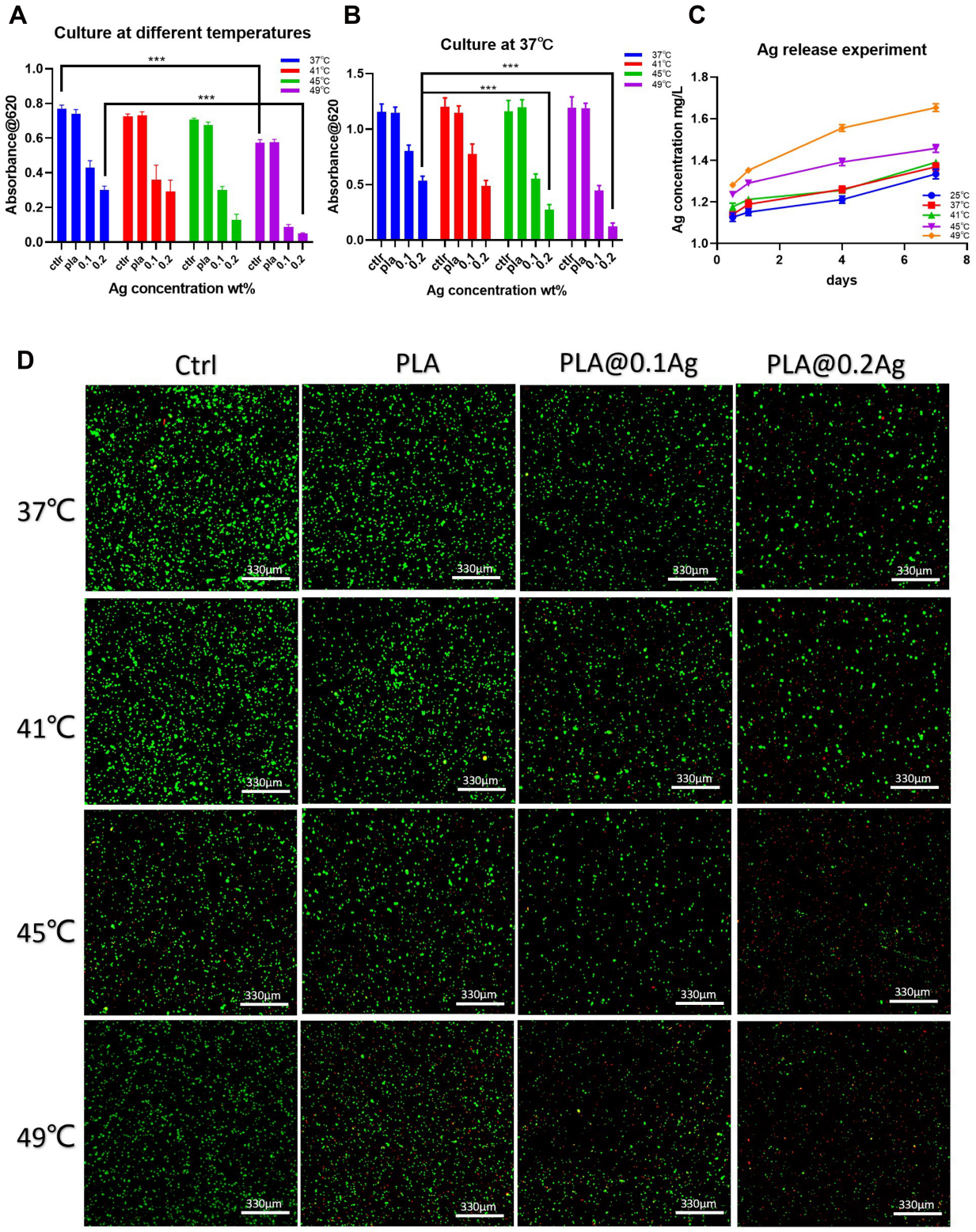

Figure 4 Antibacterial properties of APA multifunctional coating under different temperatures. (**A**) UV absorption spectrum at 620nm of bacterial liquid co-culture with different PLA@Ag film at different temperature (37°C, 41°C, 45°C, 49°C), respectively. (**B**) UV absorption spectrum at 620nm of bacterial liquid co-culture with different PLA@Ag film at 37°C (pretreated at 37°C, 41°C, 45°C, 49°C), respectively. (**C**) Ag release experiment for PLA@0.2Ag film at different temperature (25°C, 37°C, 41°C, 45°C, 49°C). (**D**) Live & dead bacterial viability under a fluorescence microscope after co-culture with different PLA@Ag film at different temperature (37°C, 41°C, 45°C, 49°C). ***p< 0.001.

silver ions in the coating were released into the tissues that cooperate with the high temperature to play an excellent bactericidal effect, because under the high-temperature environment. Therefore, the same method of in vitro heating was used to treat infections of metal implants. After being coated with APA multifunctional coating, it could achieve the ideal antibacterial effect without heating to a high temperature of 60°C, which significantly reduces thermal damage to the tissue. Therefore, the APA multifunctional coating not only had an excellent antibacterial effect in regular use but also improved the germicidal ability of the coating, thus reducing the incidence of metal implant infection through the method of electromagnetic heating in vitro when necessary.

Thermal Insulation Effect of PLA@Ag Film

In order to evaluate the thermal insulation effect of APA multi-functional coating with different concentrations and particle size of AgNPs, the infrared camera was used to photograph the heating performance of different films in a 50°C constant temperature water bath. The results are displayed in Figure 5A and B. From the thermal image, PLA@Ag composite film did have an excellent thermal insulation effect. The initial temperature of PLA@Ag composite film was significantly lower than that of pure PLA film and the ambient temperature. Moreover, the thermal insulation ability increased significantly with the increase of AgNPs concentration and particle size. From the heating curve illustrated in Figure 5C and D, the first 20 seconds was the rapid temperature rising period. The temperature difference among the groups reached the maximum at about 20 seconds. Then, temperature increased slowly and tended to be stable in the 20s-40s period. The surface temperature of each group was stable and decreased slowly with the water temperature after 40 seconds. The temperature in the water bath was about 49.2°C in about 20s. At 20s, compared with water, the temperature difference (Δ T) of pure PLA film was 1.6°C, and PLA@0.1Ag, PLA@0.2Ag, PLA@0.3Ag, PLA@0.4Ag were 3.6°C, 3.8°C, 4.3°C, and 5°C, respectively. As mentioned earlier, for human bodies, there are usually three ways of heat transfer, heat conduction, convection, and radiation at a given temperature that must be able to reduce unnecessary heat exchange with the surrounding environment in these three aspects.[23,24] Therefore, in order to explore the influence reason of the AgNPs with different concentrations and particle size on the thermal insulation effect, we evaluated in detail the thermal conductivity and infrared radiation reflectivity of each PLA@Ag composite films. As shown in Figure 4E, the thermal conductivity of pure PLA material was about 0.32±0.02 W·m-1·K-1, so pure PLA material was an excellent thermal insulation material, which was consistent with the conclusions of other researchers, and is one of the reasons why we chose PLA as the main body of APA multifunctional coating[56.42] However, the thermal conductivity of the composites increased slightly after the addition of AgNPs, and the higher the content of AgNPs in the composites was, the higher the thermal conductivity was. The thermal conductivity of PLA@0.4Ag was about 0.42 ±0.006W·m-1·K-1 that was 131.3% higher than that of pure PLA. With the increase of the particle size of AgNPs, the thermal conductivity of the composites also increased. Containing 100nm AgNPs with a concentration of 0.3wt %, the thermal conductivity of PLA@100Ag composites was 0.45±0.035 W·m-1·K-1 that was 140.6% higher than that of pure PLA (Figure 5E and F).

What is more, with different concentrations and particle sizes, the results of infrared radiation reflectivity of AgNPs are demonstrated in Figure 5G and H. The infrared reflectivity of PLA films increased significantly after adding AgNPs, and the average reflectivity of pure PLA materials in the range of 1.5–2 μ m was 14.41%. The average reflectivity of PLA@0.1Ag was 46.50%, and, with the increase of the concentration of AgNPs, the reflectivity obviously increased. The average reflectivity of PLA@0.3Ag was 61.67% that was about 4.3 times that of pure PLA materials. For AgNPs at the same concentration, the larger the particle size of the AgNPs was, the higher the average reflectivity of the AgNPs was. When the AgNPs concentration was 0.3wt%, the average reflectivity of the PLA@Ag composite film with a particle size of 20, 50, 100nm was 61.67%, 71.86%, and 77.46%, respectively. Therefore, it was found from our study that the higher the concentration of AgNPs was, the higher the infrared radiation reflectivity was, the larger the particle size was, and the higher the infrared radiation reflectivity was. However, the thermal conductivity of PLA@Ag composite film increased with the addition of AgNPs, which may harm the thermal insulation effect of APA multifunctional coating. Based on test results, the thermal conductivity did increase, which had little effect on the thermal insulation effect of PLA@Ag composite films. Measured by the infrared camera, the actual thermal insulation effect

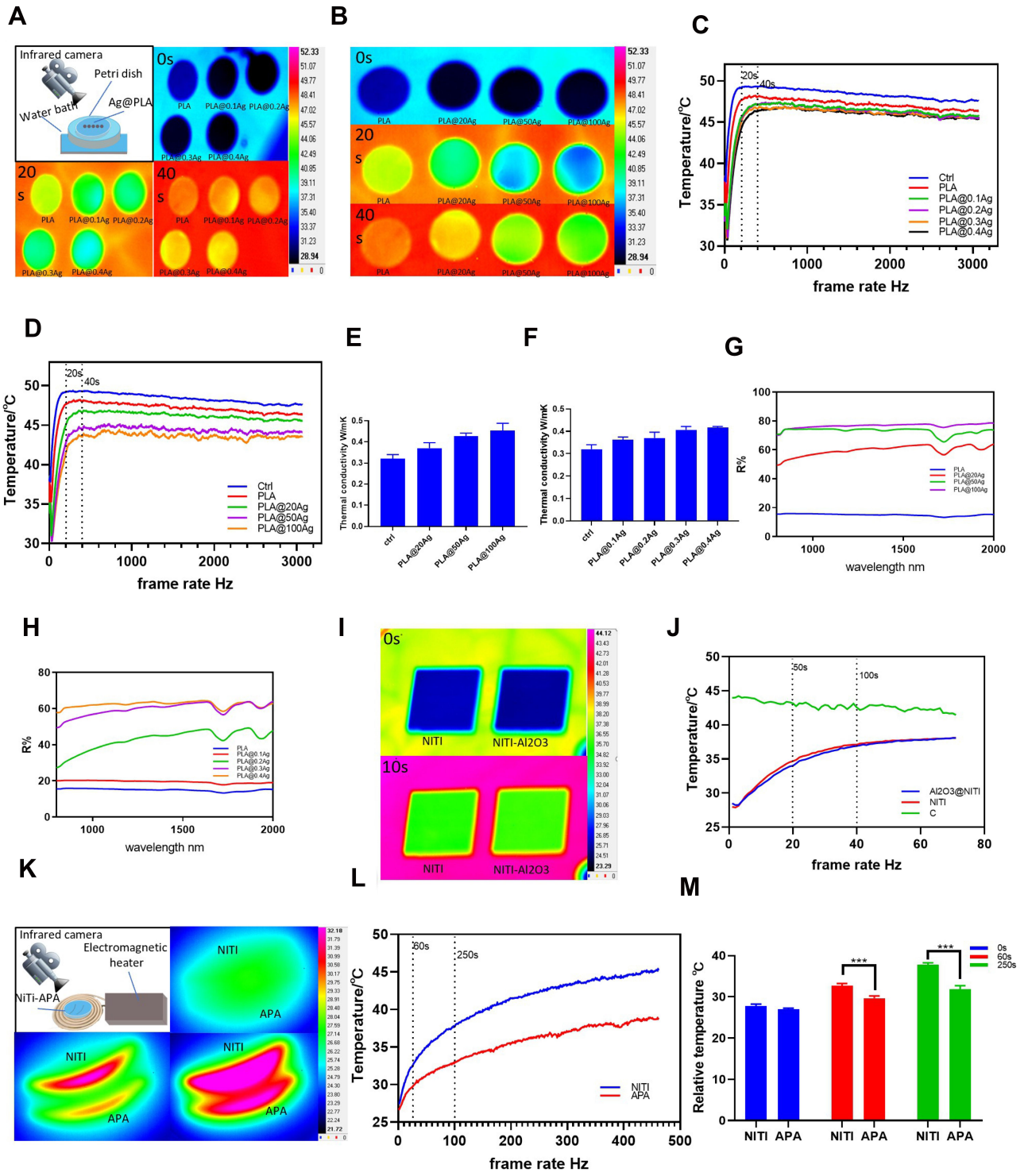

Figure 5 Thermal insulation test for APA multifunctional coating. (**A, B**) Thermal images of each sample (PLA, PLA@0.1Ag, PLA@0.2Ag, PLA@0.3Ag, PLA@20Ag, PLA@50Ag, PLA@100Ag). (**C, D**) Temperature curve for each sample (PLA, PLA@0.1Ag, PLA@0.2Ag, PLA@0.3Ag, PLA@20Ag, PLA@50Ag, PLA@100Ag, NiTi and NiTi-AL2O3). (**E, F**) Thermal conductivity of different PLA@Ag film. (**G, H**) Infrared reflectivity rates for different PLA@Ag film. (**I**) Thermal images of NiTi and NiTi-Al2O3. (**J**) Temperature curve for NiTi and NiTi-Al2O3. (**K–M**) Thermal imaging, temperature curve and surface temperature of Simulated heating in vitro for each sample (NiTi and NiTi-APA). ***p< 0.001.

was the same as the trend of infrared radiation reflectivity. The Stefan-Boltzmann law describes the thermal emission of objects. For realistic objects, the emissivity (ε) needs to be included as follows:

$J = \varepsilon \sigma T4.$

where j was the total energy flux, ε refers to the material emissivity, σ marks Stefan-Boltzmann constant, and T stans for the temperature. At the same temperature, low-emissivity materials radiate less than high-emissivity materials, so they provided more radiation insulation.[57] Therefore, the addition of AgNPs could significantly improve the infrared radiation reflection of PLA@Ag composite films, thus improving the thermal insulation ability of APA multifunctional coatings. The reason why the smaller the particle size of AgNPs is in the PLA @ Ag film had lower reflectance of infrared radiation was that as the size of the unit structure in the material decreased, the thermal conductivity decreased, and the radiant heat conduction increased. Therefore, under the premise that the thermal conductivity coefficient was not high, the larger the size is, the better the thermal insulation effect is.[58] The radiative heat conduction could increase sharply with the decrease of nano-cell size, which could be attributed to the substantial interference effect of the thin film, which significantly reduced the reflection of the infrared wave on the thin film wall. The incident infrared wave was partially reflected and absorbed when it passes through the thin film wall. Because in the case of minimal size, the thickness of the film wall was much smaller than the infrared wavelength, and the infrared waves reflected from the two interfaces may produce substantial destructive interference, thus resulting in a significant reduction in the reflectivity of the film.[59]

Thermal Insulation Effect of Al2O3 MAO Layer and APA Multifunctional Coatings

The thermal insulation effect of APA multifunctional coating depended on the synergistic effect of PLA and AgNPs and the excellent thermal insulation effect of the Al2O3 MAO layer. With low thermal conductivity, the Al2O3 oxide layer was often used to prepare composite thermal insulation materials together with other metal oxides with low thermal conductivity.[60] But the results in Figure 5I and J proved that, plated with the 20um Al2O3 oxide layer (NiTi-Al2O3), the surface temperature of SMA and SMA was not significantly different. However, according to the heating curve, the NiTi-Al2O3 was lower than that of SMA within 100s. At the 50s, the surface temperatures of NiTi-Al2O3 and SMAs were 34.57±0.16°C and 35.14 ±0.09°C, respectively, and Δ T was only 0.57°C, because the Al2O3 oxide layer in this experiment was relatively thin (20um). However, as part of the APA multi-functional coating, the Al2O3 oxide layer played a positive role in enhancing the thermal insulation effect of the PLA@Ag composite film.

From the results of thermal insulation experiment, the larger the particle size is, the higher the concentration is, and the better the thermal insulation effect of PLA@Ag composite film. However, combined with our antibacterial experimental results, the antibacterial effect decreased with the increase of the particle size of AgNPs, and the antibacterial effect of 50nm and 100nm group was much lower than that of 20nm group. Therefore, based on the versatility of APA multi-functional coating, we selected 20nm-sized AgNPs to prepare APA multi-functional coating, because the minimum concentration required for antibacterial and thermal insulation is 0.3wt% at the same time. Finally, PLA@Ag composite film composed of 20nm AgNPs with 0.3wt%, and a substrate with a thickness of 20um Al2O3 oxide layer was selected to form an APA multi-functional coating. We used agarose gel enwrapped SMA rod and APA multi-functional coating SMA rod to simulate the real thermal insulation effect of APA multi-functional coating in human tissue in vitro. Under the infrared camera, it was evident that the surface temperature of the APA group was significantly lower than that of the pure NiTi group. NiTi group not only had a high surface temperature but also had a wide heating range, and the surrounding temperature was also higher than that of the APA group. Under electromagnetic heating, the temperature difference between the two groups became larger and remained stable after 250 s until the end of 1200 s observation. The temperature difference between Δ T of APA group and NiTi group at the 60s and 250s were 3°C and 5.9°C, respectively (Figure 5K–M). The existence of APA multi-functional coating can conduct the heat produced by SMA more gently, which greatly reduces its surface temperature and prevents the thermal damage of tissue. Additionally, given by APA multi-functional coating, the longer temperature range of SMA makes SMA more widely used in human bodies without worrying about the occurrence of thermal damage.

Excellent Biocompatibility of APA Multifunctional Coating Applied to Nickel-Titanium Alloy

A large number of studies have shown that alumina ceramics, PLA, and AgNPs had excellent biocompatibility and biological activity.[61,62] Our cell proliferation experiments in vitro also proved it. The effects of extracts from pure PLA film, PLA@Ag composite film, SMA rod coated with APA multifunctional coating, and pure SMA rod on the proliferation of rat fibroblast L929 are shown in Figure 6A–C. According to CCK-8 analysis, the proliferation ability of L929 in the NITI extract group decreased

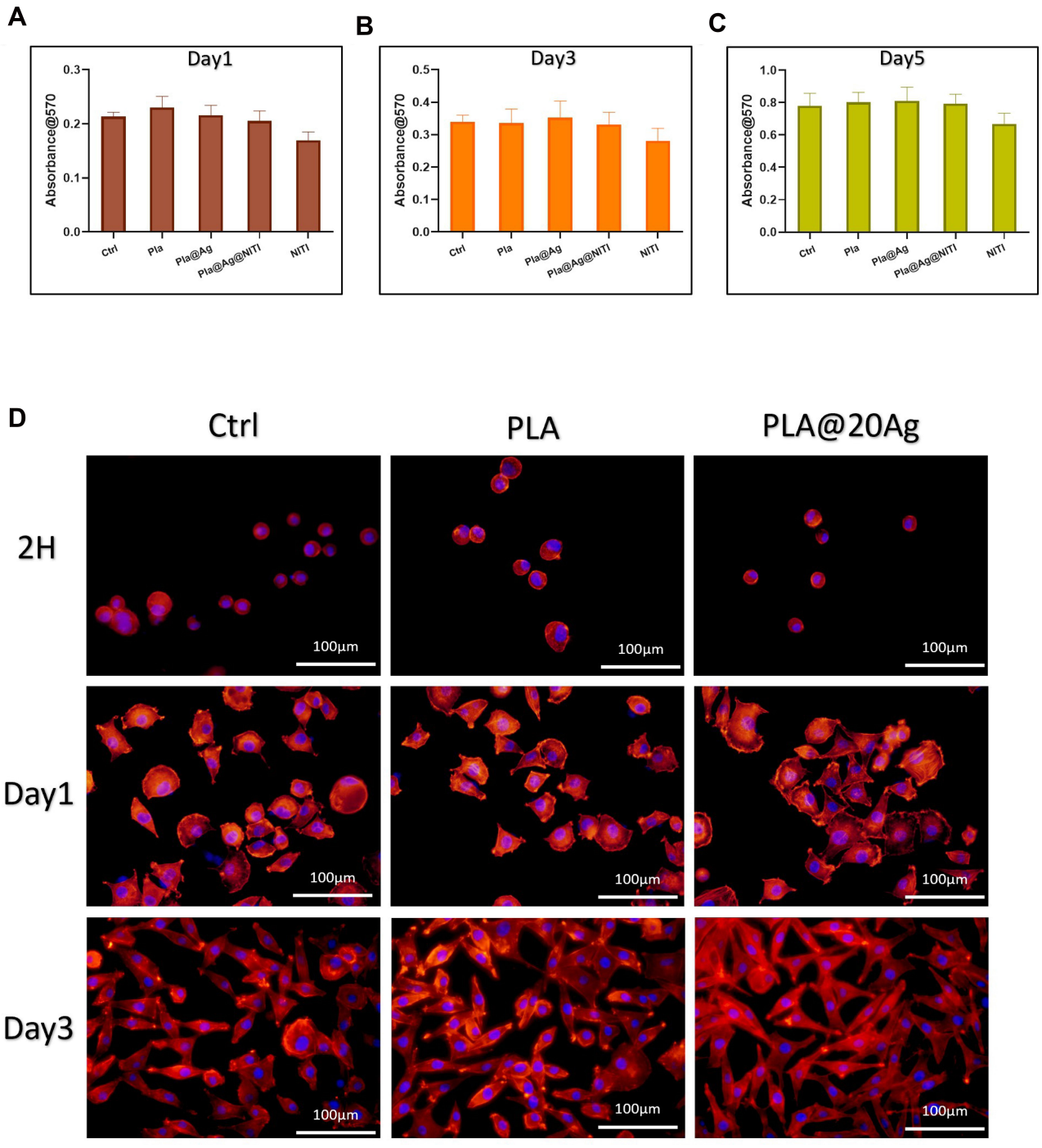

Figure 6 Excellent compatibility of APA multifunctional coating. (**A**–**C**) Viability of L929 cells incubated for 1 day, 3 days and 5 days with extracts of PLA, PLA@Ag, PLA@Ag@NiTi and NiTi. (**D**) Fluorescence microscopy images of L929 cells cultured on PLA and PLA@Ag film for 2h, 1 day and 3 days with actin stained with FITC (red) and the nucleus stained with PDAI (blue).

slightly, compared with the control group, suggesting that SMA rods had weak cytotoxicity. Meanwhile, PLA group, PLA@Ag group and PLA@Ag@NiTi group had better proliferation ability, indicating that APA multifunctional coating had excellent biocompatibility. The reason why APA coated SMA rods have better biocompatibility than pure SMA rods was that SMA rods release cytotoxic Ni ions in vivo. However, due to the shielding effect of APA multi-functional coating, the release of Ni ions and the cytotoxicity of SMA rods was reduced.

Many studies reported that the surface morphology of biomaterials was related to cell adhesion, cell growth, migration, and differentiation, which was considerably significant to biomaterials and tissue engineering.[63,64] The porosity and flatness of the material surface were the key factors that affected cell adhesion and growth. Compared with the flat surface, the surface with high porosity was more favorable for cells to form flaky lipid walls and filamentous feet, so as to adjust their structure for feeding and migration.[65] The surface of the APA multi-functional coating was embedded with a large number of AgNPs, making the surface more conducive to cell adhesion, growth, and differentiation. The morphology and proliferation of L929 cells were incubated directly on different samples, as shown in Figure 6D. As expected, compared with the control group, the composite coating sample was more suitable for cell growth. After 2 hours of culture, the L929 cells of the three groups began to adhere to the wall. After 1 day of culture, the adhesion and spreading of L929 cells on the three groups of samples were enhanced, and filamentous feet and flaky lipocytes appeared. After 3 days of culture, L929 in PLA@Ag composite film group had more filamentous pseudopodia than the control group and PLA group, and the adhesion and spreading were better than that of the control group and PLA group.

Thermal Insulation Effect of APA Multi-Functional Coating in vivo

As shown in Figure 7A, pure SMA rods and APA-plated SMA rods were implanted into the back tissue of rabbits to verify the performance of APA multifunctional coating in vivo. The optical fiber temperature probe was fixed on SMA rods, with the sham operation group as the control group. Under the same heating conditions, the temperature curve of the NiTi group and PLA@Ag@NiTi group is displayed in Figure 7B. For a total of 120 seconds from the beginning to the end of heating, the temperature of PLA@Ag@NiTi group was lower than that of the NiTi group, and the temperature difference between them was getting larger. In Figure 7C, at the end of heating the temperature of the NiTi group and PLA@Ag@NiTi group, were about 54.55 ±0.71°C and 48.39 ±0.45°C, respectively (Δ T=6.16°C). However, it is worth noting that after stopping heating, the temperature of the NiTi group decreased rapidly, while the temperature of the PLA@Ag@NiTi group decreased slightly and was higher than that of NiTi group for 150s. In Figure 7D, more nickel ions about 63 ±4mg/mL were detected in the serum of rabbits in the NiTi group. But in the control group and PLA@Ag@NiTi group, the numbers were only 29 ±2mg/mL and 37 ±3mg/mL, respectively. Detected in the rabbit serum that was implanted with APA multifunctional coating SMA, the concentration of nickel ions was much lower than that of the pure SMA group. In practical application, APA multi-functional coating can effectively reduce the release of Ni ions and improve the biocompatibility of SMA.

The HE staining of the surrounding tissue is illustrated in Figure 7E. Compared with the control group, both NiTi group and PLA@Ag@NiTi group showed inflammatory cell infiltration and the thin layer of fibrous tissue. NiTi group had a large number of inflammatory cell infiltration, and, in muscle fiber cells, vacuoles showed signs of cell lysis. However, the inflammatory response of the PLA@Ag@NiTi group was weaker than that of the NiTi group. Only a small amount of inflammatory cells infiltrated, and the morphology of muscle fiber cells was normal. As shown in Figure 7F, the staining of IL-1β and TGF-β1 in the NiTi group was more profound than that of PLA@Ag@NiTi group and control group, indicating that the tissue cells expressed more cytokines that were related to inflammation. However, there was no significant difference between the PLA@Ag@NiTi group and the control group. Human tissue cells have poor heat tolerance, and high temperatures can kill cells through a variety of mechanisms, including necrosis, apoptosis, and patterns associated with mitotic disasters.[66] When the environment of the cell was higher than the highest temperature it could tolerate that was about 43°C, it produced a series of changes, including chromosome aberration, mitotic disturbance, cytoskeleton damage, limited membrane fluidity, and then died.[11] However, if the local part of human bodies is only slightly above the critical temperature, the process is relatively mild, and the human tissue can

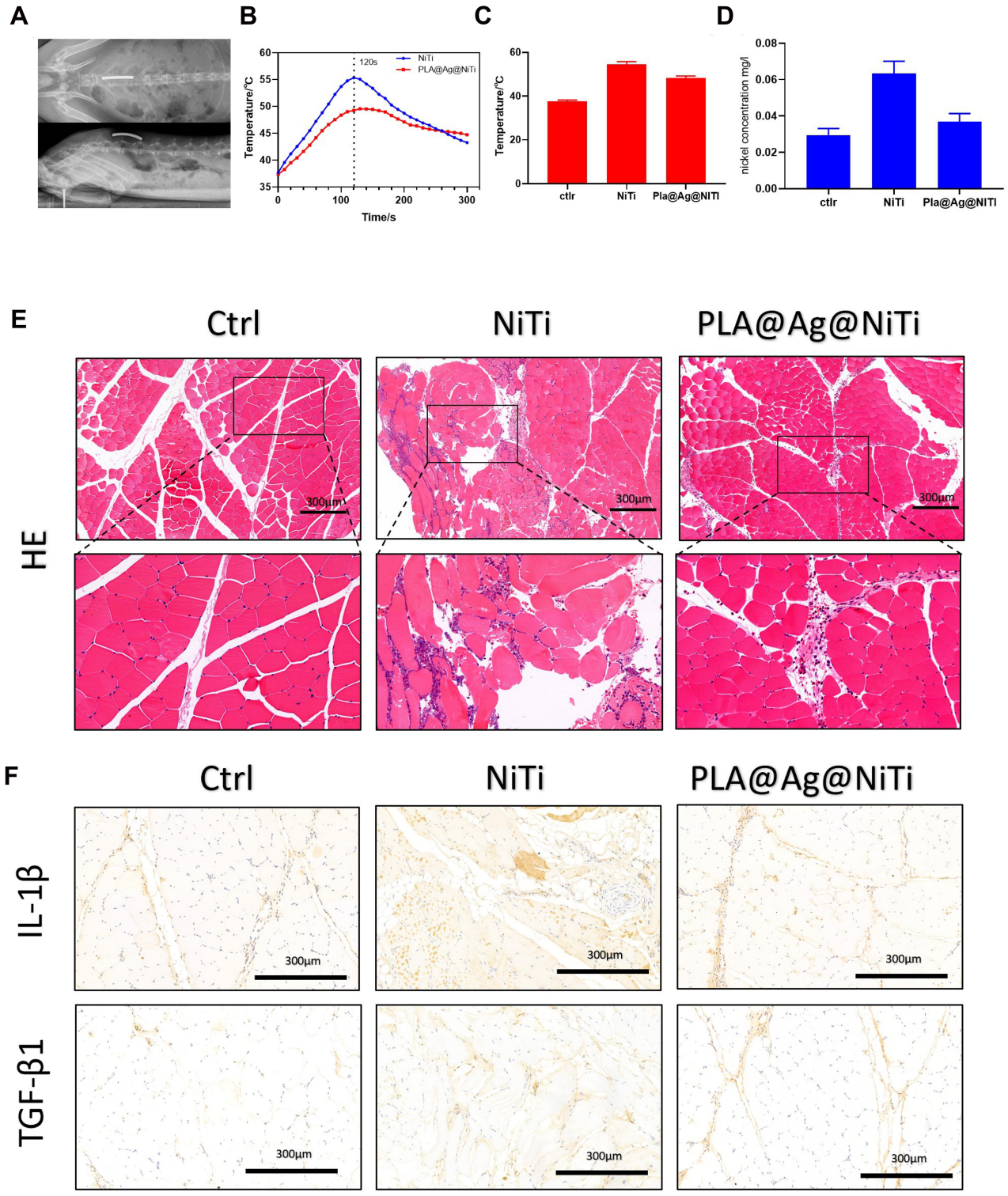

Figure 7 Actual performance of APA multifunctional coating in animals. (**A**) The x-ray diagram of the rabbit implanted with NiTi and APA@NiTi rods. (**B, C**) Temperature curve and surface temperature of NiTi and APA@NiTi rods implanted in animals by electromagnetic heating in vitro. (**D**) The concentration of Ni Ion in rabbit serum 14 days after the implantation of the material. (**E**) HE staining of muscle tissue in the sham operation group, NiTi group and APA@NiTi group 14 days after the implantation. (**F**) The Immunohistochemical staining of TGF- β1 and IL-1β for muscle tissue in the sham operation group, NiTi group and APA@NiTi group 14 days after the implantation.

tolerate it. When the local temperature was higher than 50° C, apparent tissue thermal damage occurred even for a short time, and, when the local temperature exceeds the critical temperature of 56°C, irreversible tissue thermal

damage occurred.[67] APA multifunctional coating had excellent thermal insulation ability and biocompatibility. Under the action of the alternating magnetic field, the temperature of SMA increased rapidly and reached 54.6° C, while the surface of APA multifunctional coating remained a relatively safer temperature. Therefore, we observed significant tissue damage in the NiTi group, including a large number of inflammatory cell infiltration, the release of inflammatory-related cytokines and tissue lysis. In the PLA@Ag@NiTi group, the temperature of the thermal insulation effect of APA multifunctional coating was within the range of tissue tolerance. Although there was also slight tissue damage, it did not reach the degree that human bodies could not tolerate it. Therefore, APA multifunctional coating with good corrosion resistance, biological activity, and excellent thermal insulation ability had a broad application prospect in the surface modification of metal implants in vivo, providing new sights for the study of clinical human implants.

There were still some limitations in our study. First, the particle size of the synthesized AgNPs was not uniform enough. Secondly, only gram-positive bacteria S. aureus was used for antibacterial experiments. Therefore, by our APA coating, the inhibition of other types of bacteria requires more research to illustrate. Thirdly, due to the technical limitation, and based on different particle sizes and concentrations of AgNPs, the classification of groups was still not comprehensive enough.

Conclusion

We have successfully prepared APA multi-functional coating. With high infrared reflectivity formed by AgNPs closely combined on PLA, the low thermal conductivity of AL2O3 and PLA and the infrared radiation reflection layer make APA multi-functional coating have excellent thermal insulation ability, while AgNPs give APA multi-functional coating excellent antibacterial activity. A large number of experiments reveal that, with the increase of AgNPs concentration and the increase of particle size, the silver ion release of AgNPs in APA multi-functional coating increases and decreases. Therefore, the combination of more 20nm particle size or smaller AgNPs in APA multi-functional coating can bring better antibacterial activity. In addition, the silver ion release of AgNPs also increases with the increase of temperature, so the antibacterial activity of APA multi-functional coating is also greatly enhanced by performing the function of thermal insulation. This study gives information that the higher the concentration of AgNPs is, the larger the particle size is, the higher the infrared radiation reflectivity of APA multi-functional coating is, and the better the thermal insulation effect is. In practical application, the concentration and particle size of bound AgNPs should be flexibly selected according to the actual situation. In animal and cell experiments, it can be seen that APA multi-functional coating has excellent biocompatibility, and it should be conducive to cell adhesion, so as to reduce the release of harmful substances such as nickel ions in implants, and has excellent thermal insulation ability to protect tissue from thermal damage. This makes the application of smart structure composed of SMA actuator in vivo possible and provides a broader application prospect for SMA, and has a wide application prospect in the surface modification of other human implants.

Author Contributions

All authors made a significant contribution to the work reported, whether that is in the conception, study design, execution, acquisition of data, analysis and interpretation, or in all these areas; took part in drafting, revising or critically reviewing the article; gave final approval of the version to be published; have agreed on the journal to which the article has been submitted; and agree to be accountable for all aspects of the work.

Funding

This work was supported by the Major Program of Hubei Technical Innovation Special Project, [Project No.2017ACA098], the Health Care of Yellow Crane Talent Plan of Wuhan City, [Grant No. 17], and Zhongnan Hospital of Wuhan University Science, Technology and Innovation Seed Fund Project, [Project No.znpy2016055].

Disclosure

The authors report no conflicts of interest for this work.

References

1. Leitner T, Sabirov I, Pippan R, Hohenwarter A. The effect of severe grain refinement on the damage tolerance of a superelastic NiTi shape memory alloy. *J Mech Behav Biomed Mater*. 2017;71:337–348. doi:10.1016/j.jmbbm.2017.03.020
2. Sun F, Sask KN, Brash JL, Zhitomirsky I. Surface modifications of nitinol for biomedical applications. *Colloids Surf B Biointerfaces*. 2008;67(1):132–139. doi:10.1016/j.colsurfb.2008.08.008
3. Xu JL, Zhong ZC, Yu DZ, Liu F, Luo JM. Effect of micro-arc oxidation surface modification on the properties of the NiTi shape memory alloy. *J Mater Sci Mater Med*. 2012;23(12):2839–2846. doi:10.1007/s10856-012-4755-7

4. Nematollahi M, Baghbaderani KS, Amerinatanzi A, Zamanian H, Elahinia M. Application of NiTi in assistive and rehabilitation devices: a review. *Bioengineering*. 2019;6(2).
5. Saegusa N, Sarukawa S, Ohta K, et al. Sutureless microvascular anastomosis assisted by an expandable shape-memory alloy stent. *PLoS One*. 2017;12(7):e0181520.
6. Yuan G, Bai Y, Jia Z, Hui D, Lau K. Enhancement of interfacial bonding strength of SMA smart composites by using mechanical indented method. *Compos B Eng*. 2016;106:99–106.
7. Hoang MC, Le VH, Kim J, et al. A wireless tattooing capsule endoscope using external electromagnetic actuation and chemical reaction pressure. *PLoS One*. 2019;14(7):e0219740.
8. Arab Hassani F, Mogan RP, Gammad GGL, et al. Toward self-control systems for neurogenic underactive bladder: a triboelectric nanogenerator sensor integrated with a bistable micro-actuator. *ACS Nano*. 2018;12(4):3487–3501.
9. Le BV, McVary KT, McKenna K, Colombo A. Use of magnetic induction to activate a "touchless" shape memory alloy implantable penile prosthesis. *J Sex Med*. 2019;16(4):596–601.
10. Lukina E, Kollerov M, Meswania J, et al. Analysis of retrieved growth guidance sliding LSZ-4D devices for early onset scoliosis and investigation of the use of nitinol rods for this system. *Spine*. 2015;40(1):17–24. doi:10.1097/BRS.0000000000000660
11. Elming PB, Sørensen BS, Oei AL, et al. Hyperthermia: the optimal treatment to overcome radiation resistant hypoxia. *Cancers*. 2019;11(1):60. doi:10.3390/cancers11010060
12. Ferraris S, Spriano S. Antibacterial titanium surfaces for medical implants. *Mater Sci Eng C*. 2016;61:965–978. doi:10.1016/j.msec.2015.12.062
13. Saud SN, Hosseinian SR, Bakhsheshi-Rad HR, et al. Corrosion and bioactivity performance of graphene oxide coating on TiNb shape memory alloys in simulated body fluid. *Mater Sci Eng C Mater Biol Appl*. 2016;68:687–694. doi:10.1016/j.msec.2016.06.048
14. Yun'an Qing LC, Li R, Liu G, et al. Potential antibacterial mechanism of silver nanoparticles and the optimization of orthopedic implants by advanced modification technologies. *Int J Nanomedicine*. 2018;13:3311. doi:10.2147/IJN.S165125
15. Hassani FA, Peh WYX, Gammad GGL, et al. A 3D printed implantable device for voiding the bladder using shape memory alloy (SMA) actuators. *Adv Sci (Weinh)*. 2017;4(11):1700143.
16. Granato R, Marin C, Gil JN, et al. Thin bioactive ceramic-coated alumina-blasted/acid-etched implant surface enhances biomechanical fixation of implants: an experimental study in dogs. *Clin Implant Dent Relat Res*. 2011;13(2):87–94. doi:10.1111/j.1708-8208.2009.00186.x
17. Jeon CJ, Lee JK, Kim ES. Effect of Al2O3 on thermal properties of 0.5CaAl2Si2O8–0.5CaMgSi2O6 glass–ceramics. *Ceram Int*. 2012;38:S557–S61. doi:10.1016/j.ceramint.2011.05.097
18. Abad B, Maiz J, Martin-Gonzalez M. Rules to determine thermal conductivity and density of anodic aluminum oxide (AAO) membranes. *J Phys Chem C*. 2016;120(10):5361–5370. doi:10.1021/acs.jpcc.6b00643
19. Yerokhin AL, Nie X, Leyland A, Matthews A, Dowey SJ. Plasma electrolysis for surface engineering. *Surf Coat Technol*. 1999;122(2–3):73–93. doi:10.1016/S0257-8972(99)00441-7
20. Bai L, Du Z, Du J, et al. A multifaceted coating on titanium dictates osteoimmunomodulation and osteo/angio-genesis towards ameliorative osseointegration. *Biomaterials*. 2018;162:154–169. doi:10.1016/j.biomaterials.2018.02.010
21. Shameli K, Ahmad MB, Yunus WMZW, et al. Silver/poly (lactic acid) nanocomposites: preparation, characterization, and antibacterial activity. *Int J Nanomedicine*. 2010;5:573–579. doi:10.2147/IJN.S12007
22. Spinelli G, Lamberti P, Tucci V, et al. Nanocarbon/poly(lactic) acid for 3D printing: effect of fillers content on electromagnetic and thermal properties. *Materials*. 2019;12(15):2369. doi:10.3390/ma12152369
23. Dai WJ, Gan YX, Hanaor D. Effective thermal conductivity of submicron powders: a numerical study. *Appl Mech Mater*. 2016;846:500–505. doi:10.4028/www.scientific.net/AMM.846.500
24. Zhao S, Qiu LY, Liu S. Preparation and performance study of reflection heat preservation insulation coating. *Adv Mat Res*. 2010;150–151:620–625. doi:10.4028/www.scientific.net/AMR.150-151.620
25. Tang J, Thakore V, Ala-Nissila T. Plasmonically enhanced reflectance of heat radiation from low-bandgap semiconductor microinclusions. *Sci Rep*. 2017;7(1):5696. doi:10.1038/s41598-017-05630-4
26. Xie T, He Y-L, Hu Z-J. Theoretical study on thermal conductivities of silica aerogel composite insulating material. *Int J Heat Mass Transf*. 2013;58(1):540–552.
27. Wijewardane S, Goswami DY. A review on surface control of thermal radiation by paints and coatings for new energy applications. *Renew Sust Energ Rev*. 2012;16(4):1863–1873. doi:10.1016/j.rser.2012.01.046
28. Slovick BA, Baker JM, Flom Z, Krishnamurthy S. Tailoring diffuse reflectance of inhomogeneous films containing microplatelets. *Appl Phys Lett*. 2015;107(14):141903. doi:10.1063/1.4932576
29. Smith GB. Green nanotechnology: solutions for sustainability and energy in the built environment. *J Nanophotonics*. 2011;5(1):050201. doi:10.1117/1.3562980
30. Gao G, Shi J-W, Fan Z, Gao C, Niu C. MnM2O4 microspheres (M=Co, Cu, Ni) for selective catalytic reduction of NO with NH3: comparative study on catalytic activity and reaction mechanism via in-situ diffuse reflectance infrared Fourier transform spectroscopy. *Chem Eng J*. 2017;325:91–100. doi:10.1016/j.cej.2017.05.059
31. Palmieri V, Bugli F, Lauriola MC, et al. Bacteria meet graphene: modulation of graphene oxide nanosheet interaction with human pathogens for effective antimicrobial therapy. *ACS Biomater Sci Eng*. 2017;3(4):619–627. doi:10.1021/acsbiomaterials.6b00812
32. Qing Y, Cheng L, Li R, et al. Potential antibacterial mechanism of silver nanoparticles and the optimization of orthopedic implants by advanced modification technologies. *Int J Nanomedicine*. 2018;13:3311–3327.
33. Alavi M, Rai M. Recent advances in antibacterial applications of metal nanoparticles (MNPs) and metal nanocomposites (MNCs) against multidrug-resistant (MDR) bacteria. *Expert Rev Anti Infect Ther*. 2019;17(6):419–428. doi:10.1080/14787210.2019.1614914
34. Kędziora A, Speruda M, Krzyżewska E, Rybka J, Łukowiak A, Bugla-Płoskońska G. Similarities and differences between silver ions and silver in nanoforms as antibacterial agents. *Int J Mol Sci*. 2018;19(2):444. doi:10.3390/ijms19020444
35. Alavi M, Karimi N. Antiplanktonic, antibiofilm, antiswarming motility and antiquorum sensing activities of green synthesized Ag–TiO2, TiO2–Ag, Ag–Cu and Cu–Ag nanocomposites against multi-drug-resistant bacteria. *Artif Cells Nanomed Biotechnol*. 2018;46(sup3):S399–S413. doi:10.1080/21691401.2018.1496923
36. Alavi M, Karimi N, Valadbeigi T. Antibacterial, antibiofilm, antiquorum sensing, antimotility, and antioxidant activities of green fabricated Ag, Cu, TiO2, ZnO, and Fe3O4 NPs via protoparmeliopsis muralis lichen aqueous extract against multi-drug-resistant bacteria. *ACS Biomater Sci Eng*. 2019;5(9):4228–4243. doi:10.1021/acsbiomaterials.9b00274
37. Ferdous Z, Nemmar A. Health impact of silver nanoparticles: a review of the biodistribution and toxicity following various routes of exposure. *Int J Mol Sci*. 2020;21(7):2375. doi:10.3390/ijms21072375
38. Sl S, Atya K, Neha H, Rakesh K. In vivo interactions of nanosized titania anatase and rutile particles following oral administration. *Nano Prog*. 2020;2(3):11–20.
39. Riau AK, Aung TT, Setiawan M, et al. Surface immobilization of nano-silver on polymeric medical devices to prevent bacterial biofilm formation. *Pathogens*. 2019;8(3):93. doi:10.3390/pathogens8030093
40. Rhim JW, Mohanty AK, Singh SP, Ng PKW. Effect of the processing methods on the performance of polylactide films: thermocompression versus solvent casting. *J Appl Polym Sci*. 2010;101(6):3736–3742.

41. Sarwar MS, Niazi MBK, Jahan Z, Ahmad T, Hussain A. Preparation and characterization of PVA/nanocellulose/Ag nanocomposite films for antimicrobial food packaging. *Carbohydr Polym*. 2018;184:453–464.
42. Yue X, Zhang T, Yang D, et al. Ag nanoparticles coated cellulose membrane with high infrared reflection, breathability and antibacterial property for human thermal insulation. *J Colloid Interface Sci*. 2019;535:363–370.
43. Sun Y, Xia Y. Shape-controlled synthesis of gold and silver nanoparticles. *Science*. 2002;298(5601):2176–2179.
44. Yang C, Tang Y. Preparation of silver nanowires via a rapid, scalable and green pathway. *J Mater Sci Technol*. 2015;31(1):16–22.
45. Da Silva EC, Da Silva MGA, Meneghetti SMP, et al. Synthesis of colloids based on gold nanoparticles dispersed in castor oil. *J Nanopart Res*. 2008;10(1):201–208.
46. Xu X, Yang Q, Wang Y, Yu H, Chen X, Jing X. Biodegradable electrospun poly (L-lactide) fibers containing antibacterial silver nanoparticles. *Eur Polym J*. 2006;42(9):2081–2087.
47. Gu YW, Tay BY, Lim CS, Yong MS. Biomimetic deposition of apatite coating on surface-modified NiTi alloy. *Biomaterials*. 2005;26(34):6916–6923.
48. Gu YW, Tay BY, Lim CS, Yong MS. Characterization of bioactive surface oxidation layer on NiTi alloy. *Appl Surf Sci*. 2005;252 (5):2038–2049.
49. Kalaivani R, Maruthupandy M, Muneeswaran T, et al. Synthesis of chitosan mediated silver nanoparticles (Ag NPs) for potential antimicrobial applications. *Front Lab Med*. 2018;2(1):30–35.
50. Scavone M, Armentano I, Fortunati E, et al. Antimicrobial properties and cytocompatibility of PLGA/Ag nanocomposites. *Materials*. 2016;9(1):37.
51. Kostic D, Vukasinovic-Sekulic M, Armentano I, Torre L, Obradovic B. Multifunctional ternary composite films based on PLA and Ag/alginate microbeads: physical characterization and silver release kinetics. *Mater Sci Eng C*. 2019;98:1159–1168.
52. Khatami M, Varma RS, Zafarnia N, Yaghoobi H, Sarani M, Kumar VG. Applications of green synthesized Ag, ZnO and Ag/ZnO nanoparticles for making clinical antimicrobial wound-healing bandages. *Sustain Chem Pharm*. 2018;10:9–15.
53. Wijnhoven SWP, Peijnenburg WJGM, Herberts CA, et al. Nano-silver – a review of available data and knowledge gaps in human and environmental risk assessment. *Nanotoxicology*. 2009;3 (2):109–138.
54. Taglietti A, Arciola CR, D'Agostino A, et al. Antibiofilm activity of a monolayer of silver nanoparticles anchored to an amino-silanized glass surface. *Biomaterials*. 2014;35(6):1779–1788.
55. Pijls BG, Sanders I, Kuijper EJ, Nelissen R. Segmental induction heating of orthopaedic metal implants. *Bone Joint Res*. 2018;7 (11):609–619.
56. Weiss K-P, Bagrets N, Lange C, Goldacker W, Wohlgemuth J, editors. *Thermal and Mechanical Properties of Selected 3D Printed Thermoplastics in the Cryogenic Temperature Regime*. IOP Publishing; 2015.
57. Hsu P-C, Liu X, Liu C, et al. Personal thermal management by metallic nanowire-coated textile. *Nano Lett*. 2015;15(1):365–371.
58. Wang G, Wang C, Zhao J, Wang G, Park CB, Zhao G. Modelling of thermal transport through a nanocellular polymer foam: toward the generation of a new superinsulating material. *Nanoscale*. 2017;9 (18):5996–6009.
59. Wang G, Wang L, Mark LH, et al. Ultralow-threshold and lightweight biodegradable porous PLA/MWCNT with segregated conductive networks for high-performance thermal insulation and electromagnetic interference shielding applications. *ACS Appl Mater Interfaces*. 2018;10(1):1195–1203.
60. Salvini VR, Luz AP, Pandolfelli VC. High temperature Al2O3-CA6 insulating foamed ceramics: processing and properties. *Interceram*. 2012;61(6):335–339.
61. Alippilakkotte S, Kumar S, Sreejith L. Fabrication of PLA/Ag nanofibers by green synthesis method using momordica charantia fruit extract for wound dressing applications. *Colloids Surf a Physicochem Eng Asp*. 2017;529:771–782.
62. Formentín P, Catalán Ú, Pol L, Fernández-Castillejo S, Solà R, Marsal LF. Collagen and fibronectin surface modification of nanoporous anodic alumina and macroporous silicon for endothelial cell cultures. *J Biol Eng*. 2018;12(1):1–9.
63. Yang K, Jung K, Ko E, et al. Nanotopographical manipulation of focal adhesion formation for enhanced differentiation of human neural stem cells. *ACS Appl Mater Interfaces*. 2013;5 (21):10529–10540.
64. Liu W, Li Y, Wang T, et al. Elliptical polymer brush ring array mediated protein patterning and cell adhesion on patterned protein surfaces. *ACS Appl Mater Interfaces*. 2013;5(23):12587–12593.
65. Formentín P, Catalán Ú, Fernández-Castillejo S, et al. Human aortic endothelial cell morphology influenced by topography of porous silicon substrates. *J Biomater Appl*. 2015;30(4):398–408.
66. Vertrees RA, Das GC, Coscio AM, Xie J, Zwischenberger JB, Boor PJ. A mechanism of hyperthermia-induced apoptosis in ras-transformed lung cells. *Mol Carcinog*. 2005;44(2):111–121.
67. Eriksson AR, Albrektsson T. Temperature threshold levels for heat-induced bone tissue injury: a vital-microscopic study in the rabbit. *J Prosthet Dent*. 1983;50(1):101–107.